Applied Catalysis B: Environmental 202 (2017) 539–549

Contents lists available at ScienceDirect

Applied Catalysis B: Environmental

journal homepage: www.elsevier.com/locate/apcatb

Removal of nitrate and simultaneous hydrogen generation through photocatalytic reforming of glycerol over "in situ" prepared zero-valent nano copper/P25

Roberta Lucchetti[a], Luca Onotri[b], Laura Clarizia[a], Francesco Di Natale[a], Ilaria Di Somma[c], Roberto Andreozzi[a], Raffaele Marotta[a,*]

[a] Dipartimento di Ingegneria Chimica, dei Materiali e della Produzione Industriale, Università di Napoli Federico II, P.le V. Tecchio 80, 80125 Napoli, Italy
[b] Centro Interdipartimentale di Ricerca Ambiente, Università di Napoli Federico II, via Mezzocannone 16, 80136 Napoli, Italy
[c] Istituto di Ricerche sulla Combustione, Centro Nazionale delle Ricerche IRC-CNR, p.le V. Tecchio 80, 80125 Napoli, Italy

ARTICLE INFO

Article history:
Received 14 July 2016
Received in revised form
14 September 2016
Accepted 22 September 2016
Available online 24 September 2016

Keywords:
Nitrate removal
Hydrogen generation
Photoreforming
Sacrificial photocatalysis
Copper loaded-TiO_2

ABSTRACT

The photocatalytic reduction of nitrate to nitrogen and the simultaneous production of hydrogen was investigated over copper loaded titania (P25) nanoparticles using glycerol as sacrificial agent and UV-A/Vis radiation. The experiments demonstrated that total nitrogen (i.e., nitrate, nitrite, and ammonia) removal efficiencies over 93% were achieved for initial nitrate concentrations up to 150 mg/l. A parallel hydrogen production up to 14 μM was recorded. Hydrogen generation was affected by nitrate reduction. The reaction rates were dependent on pH and both glycerol and nitrate starting concentrations in the mixture. However, a linear model can be used to describe the process for low concentration of nitrate and constant pH. The system showed a remarkable photoefficiency in decontamination of nitrate-containing solutions and concomitant hydrogen evolution. This study lays the foundation for the future development of numerical models able to predict the chemical behavior of simultaneous proton and nitrate reduction over solar photocatalytic reforming of organics.

1. Introduction

Nitrate is one the most abundant ground and surface-water contaminants due to the massive use of fertilizers in agricultural activities, the disposal in the environment of large amounts of livestock manure, and the discharge of not efficiently treated wastewater [1]. Nitrate contamination is potentially hazardous to human health since it can cause methemoglobinemia (also known as "blue baby" syndrome), a highly fatal disease in babies under 6 months of age [2]. Nitrate ions are also considered endocrine disrupting chemicals with carcinogenic effects [3], leading to the production of nitrosamines in the human body [4]. For this reason, many Countries limited the nitrate content in drinking, ground, and surface water through specific regulations [5].

Conventional processes for the remediation of nitrate-contaminated ground waters such as biological processes, electro-kinetic denitrification, reverse osmosis, ion exchange and chemical reduction are often adopted or have been proposed in the past, even if they show some drawbacks such as sludge production, relatively high operative costs and undesirable by-product formation [6].

Among all alternative technologies for nitrate removal in water, photocatalytic reduction processes are very promising for the possibility of exploiting solar energy to convert nitrate into non-toxic final by-products such as nitrogen gas instead of undesirable by-products (e.g., ammonia) that require additional treatments [49]. In particular, a large number of studies focused their attention on the photocatalytic activity of TiO_2 catalysts doped with metal ions conferring an increased nitrate removal efficiency with respect to bare TiO_2 (Table 1).

According to the literature, the presence of metal species in photocatalytic systems helps reduce the occurrence of photogenerated electrons/holes recombination and increase the charge-separation lifetime. Once transferred from the conduction band of TiO_2 to the metal, the photogenerated electrons are available for nitrate reduction.

Photocatalytic nitrate reduction is normally carried out under deaerated conditions and in presence of organic molecules acting as hole scavengers in order to increase the efficiency. As reported in Table 1, most of the papers found in the literature review were

* Corresponding author.
E-mail address: rmarotta@unina.it (R. Marotta).

http://dx.doi.org/10.1016/j.apcatb.2016.09.043
0926-3373/

Table 1
Literature information on TiO_2-photocatalytic reduction of nitrate.

Photocatalyst and preparation method	Hole scavenger	Photocatalyst concentration *(g/l)*	Photocatalyst activity ($mmol_{NO_3^-}/min\,g_{photocatalyst}$)	$X_{NO_3^-}$ and treatment time *(%, h)*	S_{N_2} *(%, h)*	Intermediates and final products *(measured)*	Ref
TiO_2 (P25, Hombikat UV100) (commercial)	Formic acid	1	–	64–77 (n.r)	n.r.	NO_2^-, NH_3	[7]
TiO_2 (P25, Kronos-1002) (commercial)	Humic acids	0.1	–	43 (66)	n.r.	n.r.	[8]
TiO_2 (P25, Hombikat UV100) (commercial)	Formic acid	0.4	$1.6{\cdot}10^{-1}$	100 (0.25)	55–58 (0.25)	NO_2^-, NH_3	[9]
TiO_2 (Hombikat UV100) (commercial)	Formic acid	1	$9.20{\cdot}10^{-4}$	87 (2)	71 (2)	NO_2^-, NH_3	[10]
TiO_2 (P25) (commercial)	Oxalic acid	2.5	–	≈ 3 (4)	n.r.	NO_2^-, NH_3	[11]
TiO_2 (P25) (commercial)	Formic acid	1	$8.80{\cdot}10^{-4}$	27 (4)	72	NO_2^-, NH_3	[12]
Cu-Pd/TiO_2 (P25) (impregnation and calcination)	Formic acid	15	$2.2{\cdot}10^{-3}$	100 (1)	n.r.	NO_2^-, NH_3	[13]
Cu-Pd/TiO_2 (P25) (impregnation and calcination)	Formic acid	2	$1.5{\cdot}10^{-2}$	84 (4)	83 (4)	NO_2^-, NH_3	[14]
Pd/TiO_2 (P25) (impregnation, reduction and calcination)	Formic acid	0.6	$5.0{\cdot}10^{-2}$	70 (4)	56 (0.33)	NO_2^-, NH_3	[15]
Cu-Pd/TiO_2 (impregnation, reduction and heating)	Formic, oxalic acids, methanol, ethanol	0.5	$5.4{\cdot}10^{-2}$	18–98 (4)	86–100 (1)	NO_2^-, NH_3	[16]
Cu-Pd/TiO_2; Cu-Pt/TiO_2; Cu-Ni/TiO_2 (P25) (co-impregnation/calcination)	Oxalic acid	1	$5.2{\cdot}10^{-3}$	17 (2)	19–100 (2)	NO_2^-, NH_3	[17]
Ag/TiO_2 (P25) (in situ or conventional photoreduction)	Formic acid	1	$2.2{\cdot}10^{-1}$	72–98 (0.5)	84–100 (0.5)	NO_2^-, NH_3	[18]
Ag/TiO_2 (P25) (in situ photoreduction)	Formic acid	1	–	100 (n.r)	n.r.	NO_2^-, NH_3	[19]
Ag/TiO_2 (P25) (in situ photoreduction)	Formic acid	1	–	100 (n.r)	n.r.	NO_2^-, NH_3	[20]
Ag/TiO_2 (P25) (photodeposition and calcination)	Formic acid	0.1–1.2	$7.4{\cdot}10^{-3}$	65–90 (240)	n.r.	NO_2^-, NH_3	[21]
Ag_2O/TiO_2; Ag/TiO_2 (P25) (chemical reduction)	Formic acid	1	$3.3{\cdot}10^{-3}$	70–100 (4)	37–85 (4)	NO_2^-, NH_3	[12]
Cu/$MgTiO_3$-TiO_2 (P25) (impregnation/calcination)	Sodium oxalate	1	$4.6{\cdot}10^{-3}$	39 (2)	n.r.	NO_2^-, NH_3	[22]
Cu/TiO_2; Cr/TiO_2; Zn/TiO_2 (Hombikat UV100) (photodeposition)	Formic acid	1	$1.4{\cdot}10^{-2}$	56–95 (2)	50–95 (2)	NO_2^-, NH_3	[10]
M/TiO_2 (P25); M: Ag, Au, Co, Cu, Ni, Pd, Pd (impregnation, reduction and calcination)	Oxalic acid	10	–	3–86 (3–6)	n.r.	NO_2^-, NH_3	[23]
Cu-Pt/TiO_2 (impregnation, reduction and calcination)	Benzene	1	$2.0{\cdot}10^{-3}$	67 (4)	20–80 (4)	NO_2^-, NH_3	[24]
ZnO-TiO_2 (Hombikat UV100) (photodeposition)	Formic acid	1	$1.42{\cdot}10^{-2}$	92 (2)	95 (2)	NO_2^-, NH_3	[25]
M/TiO_2 (P25, Hombikat UV100); M: Cu, Ag, Fe (impregnation or photodeposition)	Formic acid	0.4	$4.6{\cdot}10^{-2}$	100 (0.25)	11–96 (0.25)	NO_2^-, NH_3	[9]
Bi/TiO_2 (sol-gel, impregnation and calcinations)	Formic acid	1	$2.0{\cdot}10^{-3}$	83 (3)	n.r.	NO_2^-, NH_3	[26]
Au/TiO_2 (P25, Hombikat UV100); (precipitation)	Oxalic acid	0.2	$2.5{\cdot}10^{-2}$	52–60 (3)	n.r.	n.r.	[27]

devoted to the synthesis and use of TiO_2-P25 materials doped with noble and expensive metals such as Pt, Au, Pd, and Ag deposited on the TiO_2 surface through impregnation, reduction, and calcination steps. Only a few studies have been carried out by using copper as low-cost and efficient doping agent [9,10,23]. Among all preparation methods of copper modified-TiO_2 catalysts, the direct "in situ" photoreduction of cupric ions has been minimally explored by researchers [30]. Formic acid, oxalic acid, methanol or ethanol have been generally used as hole scavengers. Moreover, a quite high catalyst concentration (1 g/l) has been normally adopted in the photocatalytic experiments. On the other hand, numerous studies demonstrated that, under the same experimental conditions adopted for nitrate removal, hydrogen production through photocatalytic reforming of organics can be achieved over M/TiO_2 catalysts (M = Ag, Au, Cu, Pd, Pt) [28–30]. In particular, some of the Authors recently proved that hydrogen production through photoreforming of oxygenated species (alcohols and carboxylic acids) can be significantly enhanced with respect to bare TiO_2-P25 by using copper/P25 nanoparticles synthesized by "in situ" deposition [31,32]. The method they proposed (reductive photodeposition), unlike the impregnation method, does not require either thermal stress (calcination) or washing procedures to prepare Cu-loaded P25 nanoparticles. Moreover, the investigations, conducted using several diagnostic techniques, indicated the formation of zero-valent copper nanoparticles with a mean diameter of about 30 nm on the TiO_2 surface. The highest reaction rates were obtained for very polar organic hole scavengers, such as methanol, glycerol and formic acid, which have high affinity for the photocatalyst surface.

The present paper aims at investigating the possibility to use this photocatalyst (nano-$Cu_{(s)}$/P25) at relatively low concentration (150 mg/l) for nitrate removal from aqueous solutions and simultaneous hydrogen generation under artificial UV-A/Vis radiation. Glycerol, a major byproduct in the biodiesel manufacturing process, was selected as a model hole scavenger.

2. Material and methods

2.1. Materials

Glycerol (≥99.5%), TiO_2 nanopowder (commercial grade, Aeroxide TiO_2-P25, average particle size 21 nm, specific surface area 50 ± 15 m^2/g, 80/20 anatase/rutile), cupric sulfate pentahydrate ($CuSO_4 \cdot 5H_2O$, >98%), sodium nitrate (>99%), sodium nitrite (99%), ammonium chloride (99.5%), phenol (>99%), ethanol (>99%), sodium nitroprusside dihydrate, sodium hypochlorite and sodium citrate tribasic (>99%) were purchased from Sigma Aldrich. Bidistilled water was used for the preparation of the reacting mixtures.

2.2. Photocatalytic procedure

Experimental runs were carried out in an annular glass batch reactor (575 ml). The reactor was magnetically stirred and thermostated at 25 °C by means of a thermostatic bath (Falc GTR 90), and equipped with a high-pressure mercury lamp (Helios Italquartz, 125 W), mainly emitting in the wavelength range of 300–400 nm (manufacturer's data). On the top of the cylindrical photoreactor, an inlet allowed to feed reactants and nitrogen gas and an outlet was used to collect liquid/gaseous samples at various reaction times. The photon fluxes of the Hg-lamp were 193 W m^{-2} (λ = 300–400 nm) and 122 W m^{-2} (λ > 400 nm).

For each run a proper amount (45 mg) of P25 nanopowder was initially suspended in an aqueous mixture (300 ml) containing glycerol at fixed concentration. The pH of the mixture was not regulated.

With the aim of avoiding the trapping reaction between dissolved oxygen and photogenerated electrons, for each photocatalytic experiment, nitrogen gas was fed at a flow rate of 0.3 l/min for 30 min before the addition of cupric sulfate pentahydrate to the slurry mixture. The starting cupric ion concentration (0.24 mM) was selected on the basis of a previous paper on hydrogen production through glycerol photoreforming in presence of nano-$Cu_{(s)}$/P25 [33] and was equivalent to 10% wt% of the TiO_2-P25 amount initially added into the mixture (150 mg/l).

Sodium nitrate, sodium nitrite, or ammonium chloride were added as nitrogen source when cupric ions were completely photoreduced on the TiO_2-P25 surface (1 h after $CuSO_4 \cdot 5H_2O$ addition). The system was kept under nitrogen atmosphere throughout the photocatalytic runs to avoid the presence of air inside the reactor.

2.3. Analytical procedures

At different reaction times gaseous and liquid samples were collected by means of Tedlar gas sampling bags (1 l) and glass syringes (10 ml), respectively. Gaseous samples were analyzed by a gas-chromatograph (Agilent 7820A) equipped with a HP-PLOT Molesieve 5A column (Agilent) and a TCD detector using argon as carried gas. Liquid samples were quickly filtered on regenerated cellulose filters (pore diameter 0.20 μm, Scharlau). The filtrate was used to measure pH and concentrations of total dissolved copper, nitrate, nitrite, and ammonia.

The concentration of dissolved copper was evaluated by a colorimetric method using an analytical kit (Macherey-Nagel) based on oxalic acid bis-cyclohexylidenehydrazide (cuprizone). An UV/vis spectrophotometer (Cary 100 UV–vis Agilent) was used for the measurements at a wavelength of 585 nm. Nitrate and nitrite were analyzed using ion chromatography (883 Basic IC PLUS, Metrohm) equipped with a Metrosep A Supp 5 250/4 column (eluent: 3.2 mM sodium carbonate, 1.0 mM sodium hydrogen carbonate). Ammonia concentration was measured using a colorimetric method (indophenols blue method). The pH of the solution was controlled by means of an Orion 420 p pH-meter (Thermo). Irradiance measurements were carried out on the external wall of the reactor through a digital radiometer (Delta Ohm HD 2102.1).

Dynamic light scattering analyses (DLS) were performed by a Master Sizer 2000 granulometer (Malvern Instruments) operating with water as dispersion solvent down to a minimum particle size of 0.02 μm. DLS analysis were carried out on bare P25 only (not $Cu_{(s)}$/P25) because the device does not provide an inertization system of aqueous suspensions in order to avoid the fast reoxidation of zero-valent copper.

3. Results and discussion

3.1. Preliminary tests and rationale of the experiments

Preliminary runs, were conducted (*i*) in the dark by using nano-$Cu_{(s)}$/P25 in presence of hole scavenger, (*ii*) under radiation but in presence of bare P25 and hole scavenger, (*iii*) in presence of nano-$Cu_{(s)}$/P25 but without any organic hole scavenger.

None of these experiments exhibited nitrate consumption within 5 h of treatment. These experimental results demonstrated that both nitrate direct photolysis and nitrate adsorption on the photocatalyst can be neglected.

Experimental tests were performed to provide information on the kinetics of both nitrate reduction and the reactions of nitrate byproducts (nitrite and ammonia). For this purpose, tests were performed using nitrate, nitrite, and ammonia. Further tests were also performed at different concentrations of glycerol and nitrate.

Table 2
Activity of nano-$Cu_{(s)}$/P25 in photocatalytic reduction of nitrate and hydrogen production.

$[Glycerol]_o$ (mM)	$X_{NO_3^-}$ (%)[a]	$S_{NO_2^-}$ (%)[a]	$C_{H_2}^{max}$ (μM)	Photocatalyst activity ($mmol_{NO_3^-}/min\,g_{photocatalyst}$)[a]	Photocatalyst load (mg/l)	$C^o_{NO_3^-}$ (mg/l)[b]
0.8	29.0	75.4	2.30	$1.5{\cdot}10^{-1}$	150	48.2
8	61.3	51.3	9.90	$3.2{\cdot}10^{-1}$	150	48.9
80	88.9	50.9	12.6	$4.5{\cdot}10^{-1}$	150	47.5
800	91.1	46.2	13.7	$4.3{\cdot}10^{-1}$	150	43.5

[a] After 10 minutes of treatment time.
[b] Starting nitrate concentration.

3.2. Nitrate reduction and hydrogen production: role of the hole scavenger concentration

Table 2 shows the values obtained for nitrate conversion degree ($X_{NO_3^-}$), selectivity to nitrite ($S_{NO_2^-}$), maximum concentration of hydrogen produced ($C_{H_2}^{max}$), and photocatalyst activity at various hole scavenger concentration.

The highest nitrate conversion degree and the lowest nitrite selectivity were obtained for the highest starting concentration of glycerol. On the other hand, when the concentration of glycerol was low, at the end of the test time (300 min), the overall nitrate conversion was lower and the residual nitrite and ammonia concentrations were high, since under this condition photogenerated electron/hole recombination is favored.

However, for prolonged reaction times (>180 min), the conversion degree for nitrate and nitrite was higher than 97% in all runs, except for the photocatalytic test starting from a glycerol concentration of 0.8 mM (data not shown). This result was obtained at the lowest concentration of glycerol, and initial load of nitrate close to 0.7 mM. Taking into account the overall reaction:

$$NO_3^- + C_3H_8O_3 \rightarrow C_3H_6O_3 + NO_2^- + H_2O \quad \text{(r1)}$$

one mole of alcoholic group is selectively converted into aldehydic group for each mole of nitrate reduced to nitrite. Reaction r_1 indicates the hole scavenging action played not only by glycerol but also by chemical intermediates (i.e. glyceraldehydes, tartronic acid, glyceric acid, etc.) coming from glycerol oxidation.

The photocatalyst activity was comparable to the value recorded by others [18] who adopted expensive materials (Ag/P25) and a higher photocatalyst load (1 g/l). Moreover, the results demonstrated that the photocatalyst activity was affected by the starting concentration of glycerol.

An effect on the maximum concentration of hydrogen achieved was also recorded. In particular, $C_{H_2}^{max}$ increased with raising glycerol concentration, thus demonstrating that the initial concentration of organic sacrificial agent markedly affects hydrogen generation rate as indicated in reactions r_2 and r_3:

$$RCH_2OH + 2h^+ \rightarrow RCHO + 2H^+ \quad \text{(r2)}$$

$$2H^+ + 2e^- \rightarrow H_2 \quad \text{(r3)}$$

On the basis of the results so far collected, further experiments with initial concentration of glycerol equal to 800 mM were performed.

3.3. Nitrate reduction and hydrogen production: kinetics

The result of a typical photocatalytic experiment is shown in Fig. 1. During the first 30 min, cupric ions were completely reduced on the photocatalyst surface and hydrogen gas was produced according to the photocatalytic overall reaction r_4 (photocatalytic reforming of glycerol):

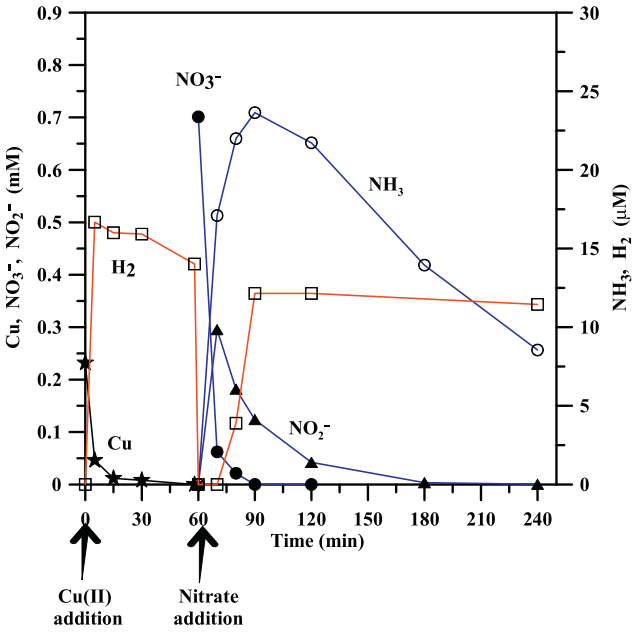

Fig. 1. Nitrate photocatalytic reduction: $[Cu(II)]_o = 0.24$ mM; C_{in} (P25) = 150 mg/l; $[NO_3^-]_o = 0.70$ mM; $[Glycerol]_o = 800$ mM. (⋆) Cu(II); (●) nitrate; (▲) nitrite; (□) hydrogen; (○) ammonia.

$$C_3H_8O_3 + 3H_2O \xrightarrow{Cu_{(s)}/P25} 3CO_2 + 7H_2 \quad \text{(r4)}$$

The addition of nitrate (1 h after starting the test) initially inhibited hydrogen generation probably due to competitive reactions of nitrate ions and protons with photogenerated electrons:

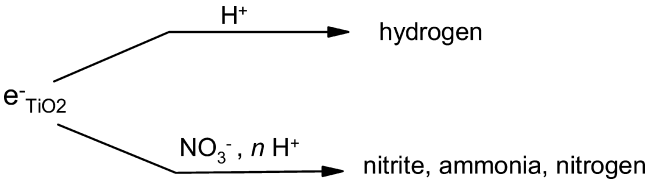

(r5)

Nitrate (0.7 mM) was mostly reduced to nitrite and only minimally to ammonia (<25 μM) within 30 min after nitrate addition, as reported in reactions r_6 and r_7:

$$NO_3^- + 2H^+ + 2e^- \rightarrow NO_2^- + H_2O \quad \text{(r6)}$$

$$NO_3^- + 9H^+ + 8e^- \rightarrow NH_3 + 3H_2O \quad \text{(r7)}$$

However, in addition to the previous reactions, the occurrence of direct conversion of nitrate to nitrogen was suggested by some literature findings [20,12]:

$$NO_3^- + 6H^+ + 5e^- \rightarrow 0.5\,N_2 + 3\,H_2O \quad \text{(r8)}$$

During nitrate reduction, a simultaneous hydrogen production up to a maximum value close to 12 μM was observed. The maximum value of hydrogen production was recorded at same time as the complete removal of nitrate, thus validating the hypothesis of competitive reactions of nitrate ions or protons with photogenerated electrons (r_5).

3.4. Tests with mixture containing nitrite

Experimental results collected through photocatalytic runs of aqueous mixtures containing only nitrite ions confirmed that the system is suitable for nitrite removal and hydrogen evolution under the same experimental conditions used for nitrate abatement (Fig. 2). A direct comparison between nitrate reduction (Fig. 1) and nitrite reduction (Fig. 2a) indicates that, within 30 min of reaction time, the rates of nitrate and nitrite removal were similar. On the other hand, when starting from nitrite, the maximum concentrations of hydrogen and ammonia, which is produced through r_9, were three/four times lower than those achieved for nitrate (Fig. 1):

$$NO_2^- + 7H^+ + 6\,e^- \rightarrow NH_3 + 2\,H_2O \quad \text{(r9)}$$

For higher reaction times, the rate of hydrogen generation in the run starting from nitrite reached a constant value similar to that observed for nitrate.

Moreover, a sharper increase in pH was also recorded for nitrite removal in the first 30 min of reaction, when the reduction of nitrate to nitrite occurred (Fig. 2b).

This result can be ascribed to the higher stoichiometric H^+/NO_2^- ratio required for nitrite reduction (r_{10}) with respect to reaction (r_6):

$$NO_2^- + 4H^+ + 3e^- \rightarrow 0.5\,N_2 + 2\,H_2O \quad \text{(r10)}$$

As a consequence, reaction (r_{10}) lowered the concentration of protons, which could generate hydrogen gas (r_3) and ammonia (r_9).

3.5. Tests with solutions containing ammonia

Similarly to nitrate and nitrite, ammonia was degraded through the photocatalytic system adopted (Fig. 3). Nitrate and nitrite were not detected during the run. Moreover, no pH deviations from a constant value of 3.2 were observed.

Poor literature results have been reported on the mechanism of photocatalytic oxidation of ammonia in presence of metal-loaded TiO_2 under deaerated conditions. Yuzawa and colleagues [34] stated that photogenered holes are able to oxidize ammonia to amide radical ($\bullet NH_2$) and proton. Amide radical further forms hydrazine (N_2H_4) which is decomposed to nitrogen and hydrogen (r_{11}):

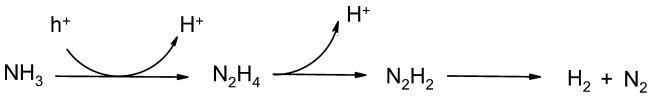

(r11)

However, Yuzawa et al. also suggested a minor route of hydrazine formation through indirect oxidation of ammonia by HO radical attack (r_{12}):

$$NH_3 + HO\cdot \rightarrow 0.5\,N_2H_4 + H_2O \quad \text{(r12)}$$

On the other hand, some literature investigations demonstrated that zero-valent copper does not form any ammonia adsorbate and is inactive for selective oxidation of ammonia [35]. Therefore, the presence of a different reaction path for ammonia oxidation should be considered. A possible mechanism involves the intervention of HO radicals, mainly generated in the reaction between water molecules and photogenerated holes (r_{13}):

$$H_2O + h^+ \rightarrow HO\cdot + H^+ \quad \text{(r13)}$$

In order to verify the occurrence of ammonia oxidation by hydroxyl radicals, the effect of *tert*-butanol, an efficient HO radical scavenger [36], was investigated. The addition of excess t-BuOH (25 mM) to the system significantly slowed down the kinetics of ammonia removal under the same conditions (Fig. 3). This result is in agreement with previous findings on the selective photooxidation of ammonia catalyzed by platinized TiO_2 [37]. However, a residual reactivity of ammonia was observed, and therefore the hypothesis of ammonia decomposition through a reaction with photogenered holes cannot be completely ruled out (r_{11}).

On the other hand, hydrogen production rate was almost unchanged regardless the presence of t-BuOH. The marginal increase in hydrogen yield recorded during the run in absence of *tert*-butanol can be ascribed to the decomposition of hydrazine (r_{11}) [34], which can also be formed through ammonia oxidation by reaction (r_{12}).

3.6. Influence of nitrate concentration

Fig. 4 shows that pH variations (full circles) accompanying nitrate reduction depend on the initial concentration of nitrate. In particular, pH increased from 3.4 to 9.3 and remained constant at this value during photocatalytic runs at high initial concentration of nitrate (518–192 mg/l). First of all, the pH value of 3.4 was attributed to the occurrence of r_2, by which two protons are formed for each alcoholic group converted [31]. The increase in pH during the photocatalytic reduction of nitrate and nitrite can be ascribed to proton consumption in reactions 6–10. For moderate starting concentrations of nitrate (43.5–93.1 mg/l), a different trend in pH was observed: after a sharp increase up to a maximum value of about 9.0, pH decreased to acidic values (4.5–5.0), once nitrate and nitrite were consumed. The decrement in pH, which started after complete removal of nitrate and nitrite ions, can be ascribed to both proton generation by reaction 2 and the presence of organic carboxylic acids [38,39]. Carboxylic acids are by-products formed through the reaction between photogenerated holes and aldehydic intermediates coming from selective oxidation of glycerol. For the lowest nitrate load (9.6 mg/l), pH was constant throughout the photocatalytic run since the molar consumption of protons was too small to induce appreciable pH changes.

The variability in pH observed at varying initial concentration of nitrate, along with the competition for adsorption on the photocatalyst surface between nitrate, nitrite, proton, and glycerol, was responsible for different selectivities and reaction rates. The reaction rates were calculated for a conversion degree of nitrate close to 90% (Table 3). In particular, pH affects:

- the adsorption capacity towards substrates of surface titanol groups on the photocatalyst (amphoteric) [41];
- the position of the flatband potential of the photocatalyst, which decreased by 59 mV per pH unit [42].

Moreover, it is noteworthy to observe that the selectivity to hydrogen decreased with increasing nitrate load, thus validating the hypothesis of (*i*) competitive surface adsorption and (*ii*) occurrence of reactions of nitrate and proton with photogenered electrons (r_5).

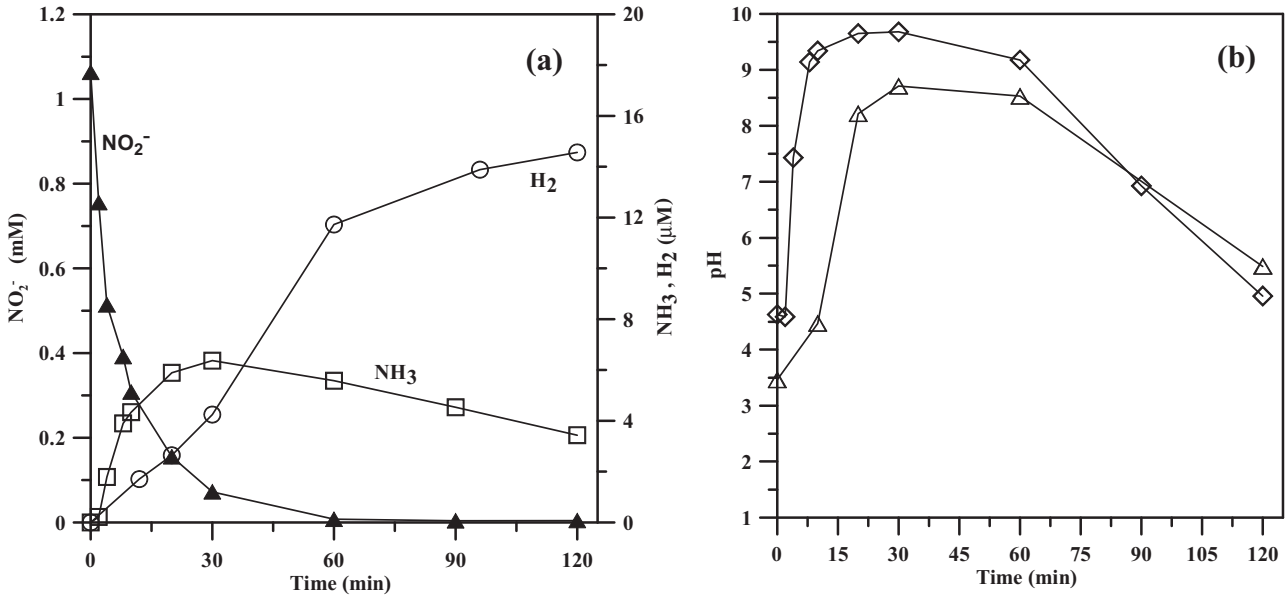

Fig. 2. (a) Nitrite photocatalytic reduction: $[Cu(II)]_o = 0.24$ mM; C_{in} (P25) = 150 mg/l; $[NO_2^-]_o = 1.06$ mM; $[Glycerol]_o = 800$ mM. (▲) nitrite; (◯) hydrogen; (□) ammonia. (b) pH change during the nitrate and nitrite photocatalytic reduction: (◊) starting from nitrite; (△) starting from nitrate.

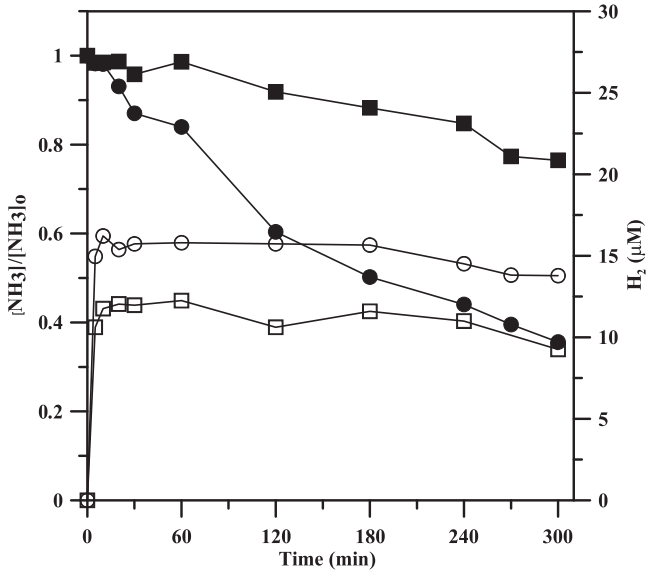

Fig. 3. Ammonia oxidation: $[Cu(II)]_o = 0.24$ mM; C_{in} (P25) = 150 mg/l; $[NH_3]_o \approx 5.00$ mM; $[Glycerol]_o = 0.8$ M. (●, ■) NH_3; (◯, □) H_2; squares (with t-BuOH, 25.0 mM), circles (without t-BuOH).

Table 3
Selectivity to nitrite, ammonia, and hydrogen for a nitrate conversion degree approximately of 90%.

$[Glycerol]_o$ *(mM)*	$X_{NO_3^-}$ *(%)*	$S_{NO_2^-}$ *(%)*	S_{NH_3} *(%)*	S_{H_2} *(%)*	Catalyst load *(mg/l)*	$C^o_{NO_3^-}$ *(mg/l)*
800	86.0	2.78	3.4	9.0	150	9.57
800	92.6	12.3	11.1	5.1	150	19.7
800	91.1	46.2	7.0	0.3	150	43.5
800	86.7	66.5	1.18	0.1	150	93.1
800	93.2	50.0	1.42	0.1	150	192
800	91.1	40.4	0.8	–	150	385
800	81.0	69.8	1.26	–	150	629

Fig. 4 also shows the specific radiative power at wavelengths lower than 400 nm transmitted during the photocatalytic process. A close link between pH and optical properties of the reacting mixture could be considered, in the sense that the transmittance decreased with increasing pH and *vice versa*. Moreover, so long as pH was constant, transmittance remained unchanged too. DLS measurements, carried out on bare P25 dispersed in different aqueous mixtures previously buffered at pH 3.5, 6.5, and 9.0, indicated uniform size distribution of the aggregates. The aggregates had a mean hydrodynamic diameter close to 2–3 μm (Fig. 5a) independent of the pH

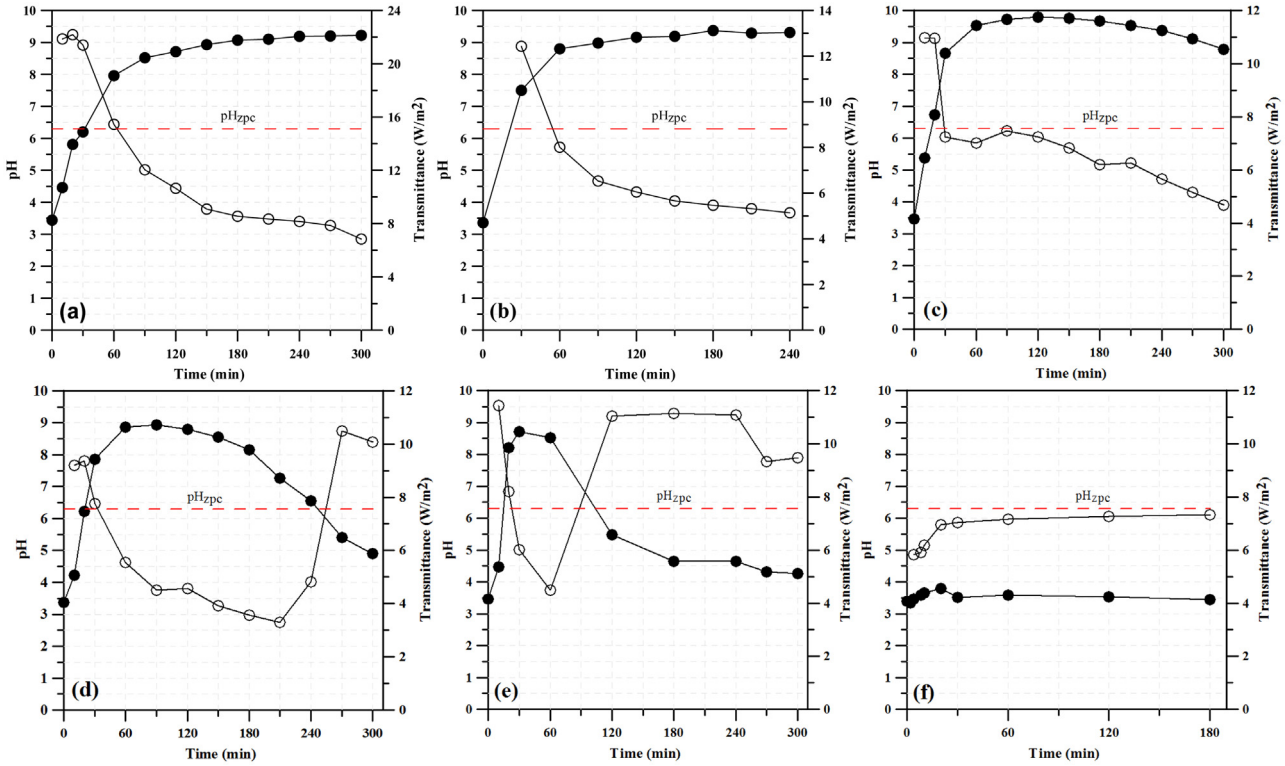

Fig. 4. pH and transmittance (λ < 400 nm) profiles: $[Cu(II)]_o$ = 0.24 mM; C_{P25} = 150 mg/l; $[Glycerol]_o$ = 800 mM. (●) pH; (○) transmittance. pH_{zpc} (P25) = 6.3 [40]. Nitrate initial concentration (mg/l): (a) 518, (b) 385, (c) 192, (d) 93.1, (e) 43.5, (f) 9.6.

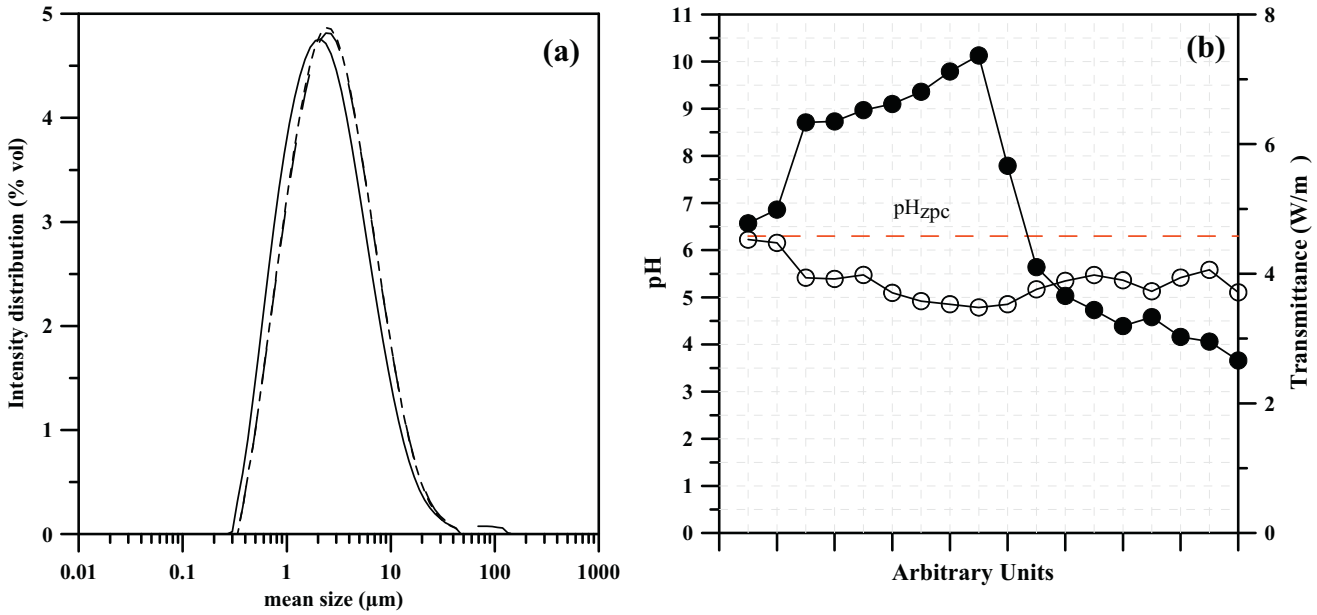

Fig. 5. (a) Laser granulometric analysis for bare P25 at different pH (continuous line pH 3.5; dashed line pH 6.5; dash-dot line pH 9.0); (b) pH and transmittance (λ < 400 nm) profiles: C_{P25} = 150 mg/l, C_{NO3} = 100 mg/l, $[Glycerol]_o$ = 800 mM. (●) pH; (○) transmittance. pH_{zpc} (P25) = 6.3 [40].

of the mixture. Additional transmittance measurements performed in aqueous mixtures at varying pH, under the same experimental conditions, indicated that the aqueous mixture did not change its optical properties if bare P25 was used instead of nano $Cu_{(s)}$/P25 (Fig. 5b).

As suggested from the collected results, the correlation between transmittance and pH should be related to different optical behaviors of metallic copper nanoparticles deposited on titanium dioxide, rather than to scattering phenomena for size changing or surface charging of bare P25. This conclusion is consistent with data reported by others [43], which observed that the pH of aqueous colloidal mixtures containing zero-valent copper nanoparticles (no TiO_2 was present) noticeably affects the UV–vis properties of the system. They related this phenomenon to a change in Cu particle size when varying pH.

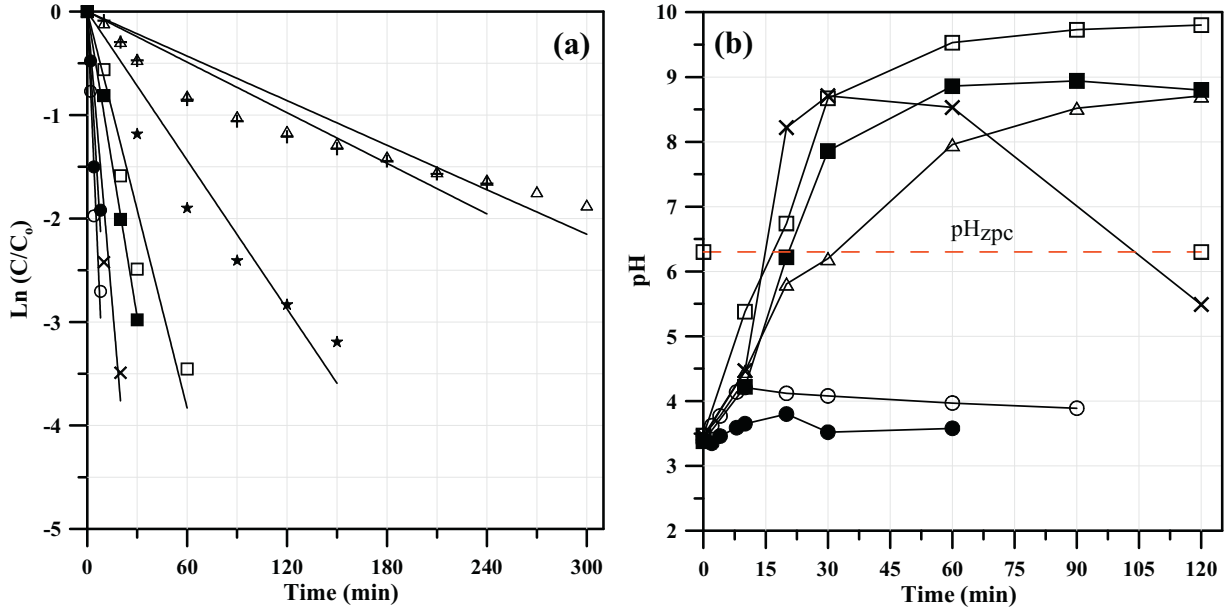

Fig. 6. (a) Pseudo-first order kinetics for nitrate removal versus reaction time; (b) $C_{NO_3^-}$ (mg/l): (●) 10, (○) 20, (✕) 44, (■) 93, (□) 150, (⋆) 385, (△) 520, (+) 630. $[Cu(II)]_o = 0.24$ mM; $C_{P25} = 150$ mg/l; $[Glycerol]_o = 800$ mM.

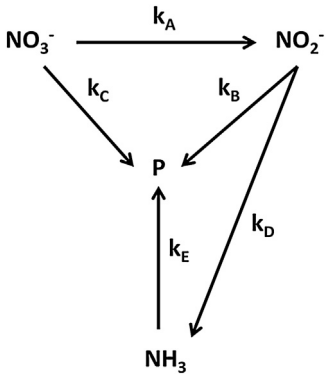

Scheme 1. Kinetic pathway proposed for the photocatalytic reduction of nitrate.

3.7. Kinetic modeling

A critical evaluation of the experimental results, together with previous literature findings [12,14,44], suggested a photocatalytic kinetic network made up of consecutive and parallel reactions for nitrate reduction. Scheme 1 shows a reaction pathway for nitrate reduction.

In the reaction network proposed, nitrate, nitrite, and ammonia were identified and measured whereas residual nitrogen containing species, such as N_2 [18,45], NO [46], N_2O, NH_2OH [47], and N_2H_4 [34] remained unknown and were generically considered as a unique pseudo-component named P. Although the reaction rates were affected by initial concentration of nitrate and pH of the mixture, at fixed photocatalyst load, a first attempt to model the system according to an apparent first order kinetics was carried out.

For this purpose, Fig. 6a shows the logarithm of normalized experimental concentration for nitrate disappearance against time. As it is clear from the figure, the hypothesis of first-order kinetics held in runs at lower nitrate concentrations (10, 20, and 44 mg/l) showing similar overall kinetic constants. For runs at nitrate loads equal to 93 mg/l and 150 mg/l, despite the first-order model only partially held, inconsistent values of kinetic constants were found. On the other hand, for highest nitrate concentrations the data clearly followed a different reaction order.

The diagrams reported in Fig. 6b show that for the runs at lower nitrate concentrations (10 and 20 mg/l), only small changes in pH were recorded during nitrate removal and, however, the highest values recorded were well below pH_{zpc} of P25 (6.3). For low nitrate concentration it can be assumed that (*i*) the proton concentration is not limiting for the photocatalytic reaction and (*ii*) the pH changes measured are not capable of significantly affecting the adsorption of substrates on the photocatalyst surface. The hypothesis of apparent first-order kinetics is therefore consistent. For an initial nitrate concentration of 44 mg/l, constant pH values far below pH_{zpc} were recorded up to a nitrate conversion of 90%. For higher nitrate concentrations, significant pH changes were recorded during nitrate removal. In this case, H_3O^+ concentration varied, so that the apparent reactions constants were expected to be different from the case of nitrate concentration equal to 10 and 20 mg/l, although linearity may still hold.

On the basis of the previous considerations, a simple first-order rate law was assumed for runs carried out at low nitrate concentrations (i.e. 10, 20, and 44 mg/l). This reaction order can be derived from simplified forms of the Langmuir–Hinshelwood-type rate law, which is generally adopted in modeling of photocatalytic processes to account for the consumption of both oxidant and reductant [25,27,33]. A first-order reaction kinetic was also proposed for the conversion of ammonia, although literature indications related this conversion to the action OH radicals generated through the oxidation of water (or hydroxyl ions) by photogenerated holes [34,37].

The kinetic constant values of the reaction pathways shown in Scheme 1 were estimated through a least-squares procedure performed with a Matlab software, applied to time course profiles of nitrogen species during the photocatalytic runs.

The numerical model uses a set of differential equations of the following type:

$$\frac{dC_i}{dt} = \sum_{k=A}^{E} \left(\pm k_j \cdot C_i\right)$$

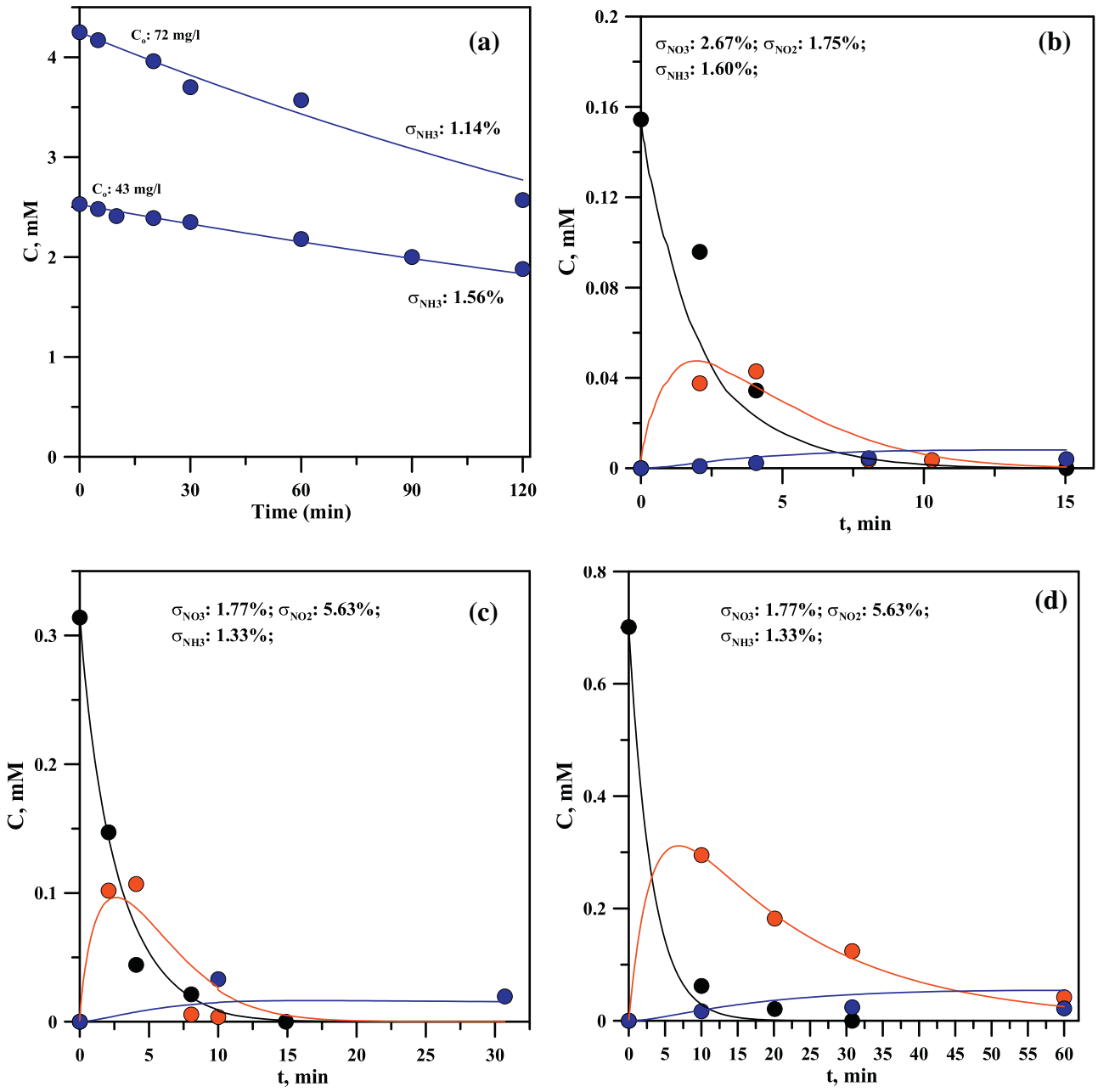

Fig. 7. Comparison between experimental (circles) and calculated (limes) concentrations. (●) nitrate, (●) nitrite, (●) ammonia. $[Cu(II)]_o = 0.24$ mM; $C_{P25} = 150$ mg/l; $[Glycerol]_o = 800$ mM. (a): $C_{ammonia} = 43$ and 72 mg/l; (b): $C_{nitrate} = 10$ mg/l; (c): $C_{nitrate} = 20$ mg/l; (d): $C_{nitrate} = 44$ mg/l. σ_j: percentage standard deviation for j-species.

where the contribution to consumption and formation of *i-th species* (C_i) is considered.

The best values for the kinetic constants (k_j) obtained with this procedure along with their uncertainties are shown in Table 4.

The first step in the modeling procedure was the evaluation of the selective oxidation of ammonia to nitrogen (Table 4, Runs n° 1 and n° 2). In particular, after estimating the parameter k_E, the model was properly modified in order to calculate the best values of the kinetic constants k_A-k_D in photocatalytic experiments at different initial concentration of nitrate (10, 20, and 44 mg/l, Table 4, runs 3–5).

At the lowest initial concentration of nitrate (10 mg/l), the reaction rate constant k_A was one order of magnitude higher than k_C, which means that nitrate was mainly converted to nitrite (r_6). Similarly, the apparent kinetic constant of nitrite reduction to unidentified nitrogen-containing compounds (k_B) was significantly higher than k_D. In other words, the reduction process of nitrite to P was kinetically favored with respect to reaction r_9. Under these experimental conditions, nitrate was in stoichiometric defect and thus unable to efficiently scavenge all free photogenerated electrons and compete with proton reduction.

At the higher initial concentration of nitrate (44 mg/l), the outcomes of the kinetic modeling suggested an increased conversion of nitrate to P (k_C) with respect to selective reduction to nitrite (k_A). These findings confirmed the expectations and clearly indicated that a more detailed kinetic modeling is required to properly describe the investigated system [33].

A comparison between predicted and measured concentrations of nitrate, nitrite and ammonia is reported in Fig. 7a–d. A good capability of the numerical model proposed to simulate the kinetic behavior of the system is evident in the diagrams.

Table 4
Apparent constant values for first-order kinetics: $[Cu(II)]_o = 0.24$ mM; $C_{P25} = 150$ mg/l; $[Glycerol]_o = 800$ mM. [(a),(b)] simultaneously calculated, [(*)] assumed from runs n° 1 and n° 2.

Run (n°)	$C_{NO_3^-}$ (mg/l)	C_{NH_3} (mg/l)	k_A (min^{-1})	k_B (min^{-1})	k_C (min^{-1})	k_D (min^{-1})	k_E (min^{-1})
1 [(a)]	–	43	–	–	–	–	$3.51\cdot10^{-3} \pm 3.00\cdot10^{-5}$
2 [(a)]	–	72	–	–	–	–	$3.51\cdot10^{-3} \pm 3.00\cdot10^{-5}$
3 [(b)]	10	–	$2.58\cdot10^{-1} \pm 3.82\cdot10^{-3}$	$2.96\cdot10^{-1} \pm 9.11\cdot10^{-3}$	$5.96\cdot10^{-2} \pm 1.62\cdot10^{-3}$	$2.12\cdot10^{-2} \pm 9.43\cdot10^{-3}$	$3.51\cdot10^{-3}$ (*)
4 [(b)]	20	–	$2.58\cdot10^{-1} \pm 3.82\cdot10^{-3}$	$2.96\cdot10^{-1} \pm 9.11\cdot10^{-3}$	$5.96\cdot10^{-2} \pm 1.62\cdot10^{-3}$	$2.12\cdot10^{-2} \pm 9.43\cdot10^{-3}$	$3.51\cdot10^{-3}$ (*)
5	44	–	$1.93\cdot10^{-1} \pm 1.05\cdot10^{-2}$	$4.29\cdot10^{-2} \pm 1.00\cdot10^{-4}$	$1.24\cdot10^{-1} \pm 8.04\cdot10^{-4}$	$7.60\cdot10^{-3} \pm 1.05\cdot10^{-4}$	$3.51\cdot10^{-3}$ (°)

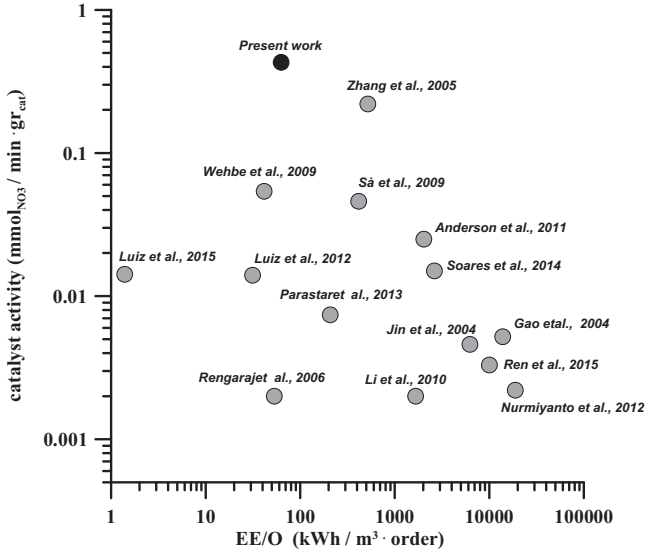

Fig. 8. Catalyst activity *vs* Electric Energy for Order. The values of catalyst activity are listed in Table 1. (●) data calculated for the run using nitrate and glycerol at initial concentrations of 43.5 mg/l and 800 mM respectively.

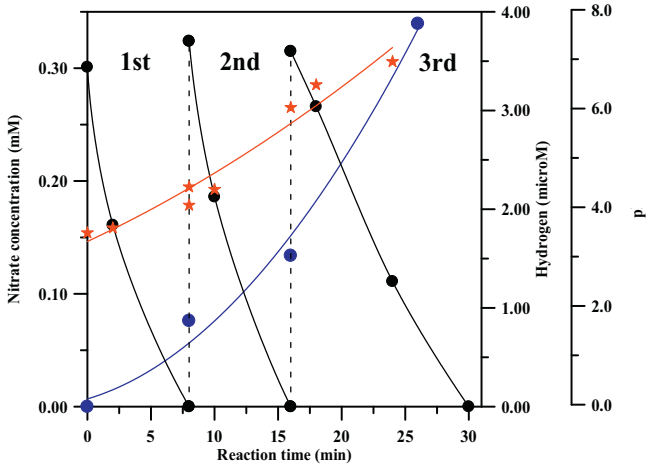

Fig. 9. Experimental outcomes from catalyst reuse: (●) NO_3^-; (●) H_2; (★) pH. $[Cu(II)]_o = 0.24$ mM; $C_{P25} = 150$ mg/l; $[Glycerol]_o = 800$ mM, $C_{nitrate} = 18.7$ mg/l.

3.8. Preliminary estimation of energy consumption

A proper figure-of-merit, named electrical energy-per-order (EE/O) [48,50], was calculated with the aim of estimating the electrical energy (kWh) required to reduce nitrate concentration by one order of magnitude per unit volume (m^3) of aqueous mixture:

$$EE/O\left(kWh \cdot m^{-3} \cdot order^{-1}\right) = 38.4 \cdot \frac{P}{V \cdot k}$$

where 38.4 is a conversion factor, P is the nominal lamp power (0.125 kW), V is the volume of solution in the reactor, and k is the overall pseudo-first-order kinetic constant (min^{-1}) of photocatalytic nitrate reduction. The parameter k was estimated through the kinetic investigation described above (for the present paper) or deduced from literature data (for previous papers).

Generally, EE/O values lower than 10 kWh m^{-3}·$order^{-1}$ are considered suitable for applications using artificial radiation [50], whereas higher values reveal a poor economic feasibility of the photoassisted process.

Fig. 8 shows values of photocatalyst activity versus EE/O for the photocatalytic reduction of nitrate over nano-$Cu_{(s)}$/P25 (present investigation) and others metal-doped TiO_2 photocatalysts reported in the literature. As is clear from the figure, the proposed system exhibited the highest photocatalyst activity ($4.3\cdot10^{-1}$ $mmol_{NO_3^-}/min{\cdot}g_{photocatalyst}$, see Table 2) among the TiO_2-based materials reported.

However, although the corresponding EE/O value (62.8 $kWh \cdot m^{-3} \cdot order^{-1}$) for the investigated system ranked amongst the lowest values deduced from literature data, it was considered far from satisfactory from the economic point of view for pre-pilot scale applications. This result may be ascribed to a non-optimal use of the energy emitted by the lamp or a limited activity of the photocatalyst at some wavelengths of the artificial radiation used.

3.9. Photocatalyst reuse

Fig. 9 shows the results of three experiments based on photocatalyst reuse. After each cycle, a new proper volume of nitrate-containing solution was added to the reactor. A very slight decrease in the photoreduction rate was observed during the 3rd recycle, probably due to small photocatalyst losses during the sampling procedure and the decrease in proton concentration. On the other hand, a continuous marked increase in hydrogen generation was recorded under the experimental conditions adopted.

4. Conclusions

Nitrate can be efficiently removed from aqueous solutions and hydrogen can be simultaneously generated through photocatalytic processes using zero-valent copper nanoparticles in situ photodeposited on P25 titania. The processes of nitrate and proton reduction develop under both acidic and alkaline conditions. However, the reaction rates are strongly affected by the hole scavenger concentration, nitrate concentration, and pH of the mixture mainly due to the proton concentration required for the photocatalytic reactions. Nitrate reduction can be described through a complex scheme of consecutive and parallel reactions in which nitrite and ammonia are formed. The selectivity to hydrogen is adversely affected by the presence of nitrate, due to the competitive adsorption processes and competitive reactions with photogenerated electrons.

The proposed system was characterized by high photocatalyst activity ($4.3\cdot10^{-1}$ $mmol_{NO_3^-}/min{\cdot}g_{photocatalyst}$) for nitrate reduction if compared with literature results. On the other hand, the corresponding value of EE/O (62.8 $kWh \cdot m^{-3} \cdot order^{-1}$) indicated that

further efforts are required for scaling-up the process to industrial applications.

Acknowledgment

The Authors are very grateful to Ing. Massimo Urciuolo (IRC-CNR) for DLS analysis.

References

[1] I. Bogardi, R.D. Kuzelka, W. Ennenga, Nitrate Contamination: Exposure, Consequence, and Control, Nato ASI Subseries G, Springer-Verlag, Berlin Heidelberg, 1991.
[2] L. Knobeloch, B. Salna, A. Hogan, J. Postle, H. Anderson, Environ. Health Perspect. 108 (2000) 675–678.
[3] J.M. Van Maanen, A. van Dijk, M.H. De Baets, P.C. Menheere, D. Van Der Heide, P.L. Mertens, J.C. Kleinjans, Toxicol. Lett. 72 (1994) 365–374.
[4] IARC, IARC Monographs on the Evaluation of Carcinogenic Risks of Chemicals to Man. Volume 17: Some N-Nitroso Compounds, World Health Organization, 1978.
[5] C. Della Rocca, V. Belgiorno, S. Meriç, Desalination 204 (2007) 46–62.
[6] A. Kapoor, T. Viraraghavan, J. Environ. Eng. 123 (4) (1997) 371–380.
[7] K. Doudrick, M. Asce, O. Monzón, A. Mangonon, K. Hristovski, P. Westerhoff P, J. Environ. Eng. 138 (8) (2012) 852–861.
[8] B. Bems, F.C. Jentoft, R. Schloègl, Appl. Catal. B: Environ. 20 (1999) 155–163.
[9] J. Sá, C.A. Aguera, S. Gross, J.A. Anderson, Appl. Catal. B: Environ. 85 (2009) 192–200.
[10] D.B. Luiz, S.L.F. Andersen, C. Berger, H.J. Jose, F.P.M. Moreira, J. Photochem. Photobiol. A: Chem. 246 (2012) 36–44.
[11] Y. Li, F. Wasgestian, J. Photochem. Photobiol. A: Chem. 112 (1998) 255–259.
[12] H.T. Ren, S.Y. Jia, J.J. Zou, S.H. Wu, X. Han, Appl. Catal. B: Environ. 176/177 (2015) 53–61.
[13] A. Nurmiyanto, H. Kondo, Y. Kamiya, Remediation of nitrate (NO_3^-) ions in groundwater by photo catalytic reduction over bimetal loaded semiconductor photo-catalysts, The 2nd International Conference on Sustainable Built Environment Publisher Universitas Islam Indonesia 7/2012.
[14] O.S.G.P. Soares, M.F.R. Pereira, J.J.M. Órfão, J.L. Faria, C.G. Silva, Chem. Eng. J. 251 (2014) 123–130.
[15] J. Sá, T. Berger, K. Föttinger, A. Riss, J.A. Anderson, H. Vinek, J. Catal. 234 (2005) 282–291.
[16] N. Wehbe, M. Jaafar, C. Guillard, J.M. Herrmann, S. Miachon, E. Puzenat, N. Guilhaume, Appl. Catal. A: Gen. 368 (2009) 1–8.
[17] W. Gao, R. Jin, J. Chen, X. Guan, H. Zeng, F. Zhang, N. Guan, Catal. Today 90 (2004) 331–336.
[18] F. Zhang, R. Jin, J. Chen, C. Shao, W. Gao, L. Li, N. Guan, J. Catal. 232 (2005) 424–431.
[19] T. Yang, K. Doudrick, P. Westerhoff, Water Res. 47 (2013) 1299–1307.
[20] K. Doudrick, T. Yang, K. Hristovski, P. Westerhoff, Appl. Catal. B: Environ. 136–137 (2013) 40–47.
[21] S. Parastar, S. Nasseri, H.S. Borji, M. Fazlzadeh, H.A. Mahvi, A.H. Javadi, M. Gholami, Desalin. Water Treat. 51 (2013) 7137–7144.
[22] R. Jin, W. Gao, J. Chen, H. Zeng, F. Zhang, Z. Liu, N. Guan, J. Photochem. Photobiol. A: Chem. 162 (2004) 585–590.
[23] H. Kominami, A. Furusho, S. Murakami, H. Inoue, Y. Kera, B. Ohtani, Catal. Lett. 76 (1–2) (2001) 31–34.
[24] L. Li, Z. Xu, F. Liu, Y. Shao, J. Wang, H. Wan, S. Zheng, J. Photochem. Photobiol. A: Chem. 212 (2010) 113–121.
[25] D.B. Luiz, H.J. José, F.P.M. Moreira, J. Chem. Technol. Biotechnol. 90 (2015) 821–829.
[26] S. Rengaraj, X.Z. Li, Chemosphere 66 (2007) 930–938.
[27] J.A. Anderson, Catal. Today 175 (2011) 316–321.
[28] G. Colon, Appl. Catal. A: Gen. 518 (2016) 48–59.
[29] A.V. Puga, Coordin. Chem. Rev. 315 (2016) 1–66.
[30] L. Clarizia, D. Spasiano, I. Di Somma, R. Marotta, R. Andreozzi, D.D. Dionysiou, Int. J. Hydrogen Energy 39 (2014) 16812–16831.
[31] L. Clarizia, I. Di Somma, R. Marotta, P. Minutolo, R. Villamaina, R. Andreozzi, Appl. Catal. A: Gen. 518 (2016) 142–149.
[32] L. Clarizia, G. Vitiello, G. Luciani, I. Di Somma, R. Andreozzi, R. Marotta, Appl. Catal. A: Gen. 518 (2016) 181–188.
[33] L. Clarizia, I. Di Somma, L. Onotri, R. Andreozzi, R. Marotta, Kinetic modeling of hydrogen generation over nano-Cu (s)/TiO_2 catalyst through photoreforming of alcohols, Catalysis Today (2016), http://dx.doi.org/10.1016/j.cattod.2016.05.053, in press.
[34] H. Yuzawa, T. Mori, H. Itoh, H. Yoshida, J. Phys. Chem. C 116 (2012) 4126–4136.
[35] A.C.A. De Vooys, M.T.M. Koper, R.A. Van Santen, J.A.R. Van Veen, J. Electroanal. Chem. 506 (2001) 127–137.
[36] S. Kim, W. Choi, Environ. Sci. Technol. 36 (2002) 2019–2025.
[37] J. Lee, H. Park, W. Choi, Environ. Sci. Technol. 36 (2002) 5462–5468.
[38] P. Panagiotopoulou, E.E. Karamerou, D.I. Kondarides, Catal. Today 209 (2013) 91–98.
[39] V. Augugliaro, H.A. Hamed El Nazer, V. Loddo, A. Mele, G. Palmisano, L. Palmisano, S. Yurdakal, Catal. Today 151 (2010) 21–28.
[40] J. Ryu, W. Choi, Sci. Technol. 42 (2008) 294–300.
[41] C. Kormann, D.W. Bahnemann, M.R. Hoffmann, Environ. Sci. Technol. 25 (1991) 494–500.
[42] M.D. Ward, J.R. White, A.J. Bard, J. Am. Chem. Soc. 105 (1) (1983) 27–31.
[43] T.M. Dung Dang, T.T. Thu Le, E. Fribourg-Blanc, M.C. Dang, Adv. Nat. Sci.: Nanosci. Nanotechnol. 2 (2011) 1–6.
[44] V. Rosca, M. Duca, M.T. De Groot, M.T.M. Koper, Chem. Rev. 109 (2009) 2209–2244.
[45] H. Kominami, T. Nakaseko, Y. Shimada, A. Furusho, H. Inoue, S.Y. Murakami, Y. Kera, B. Ohtani, Chem. Commun. 3 (2005) 2933–2935.
[46] V.N. Montesinos, N. Quici, H. Destaillats, M.I. Litter, RSC Adv. 5 (2015) 85319–85322.
[47] S. Goldstein, D. Behar, T. Rajh, J. Rabani, J. Phys. Chem. A 120 (2016) 2307–2312.
[48] J.R. Bolton, K.G. Bircger, W. Tumas, C.A. Tolman, Pure Appl. Chem. 73 (2001) 627–637.
[49] M. Shand, J.A. Anderson, Catal. Sci. Technol. 3 (2013) 879–899.
[50] J. Bolton, S. Cater, Homogeneus photodegradation of pollutants in contaminated water: an introduction, in: Surface and Aquatic Environmental Photochemistry, CRC Press, Florida, 1994, pp. 475–476.